Int. J. Electrochem. Sci., 17 **(2022)** Article Number: 220852, doi: 10.20964/2022.08.54

International Journal of
ELECTROCHEMICAL
SCIENCE
www.electrochemsci.org

Preparation of Bi/Bi_2O_3 on porous carbon cuboids for simultaneous determination of dopamine and uric acid

Zongfei Zhang[1], *Haoyong Yin*[1,*], *Heyu Zhao*[1], *Ling Wang*[2], *Jianying Gong*[1], *Qiulin Nie*[1], *Shengji Wu*[3,*]

[1] College of Materials & Environmental Engineering, Hangzhou Dianzi University, Hangzhou, 310018, China
[2] Department of Chemistry, Zhejiang Sci-Tech University, Hangzhou, 310018, China.
[3] College of Engineering, Huzhou University, 313000, Huzhou, China
[*]E-mail: yhy@hdu.edu.cn (Haoyong Yin); wushengji26@hdu.edu.cn (Shengji Wu)

Received: 18 April 2022 / *Accepted:* 9 June 2022 / *Published:* 4 July 2022

Bi/Bi_2O_3 nanoparticles were successfully deposited on the porous carbon cuboids through high temperature carbonization of bismuth-based metal organic frameworks. The as prepared Bi/Bi_2O_3/PCCs electrocatalyts were characterized by scanning electron microscopy, X-ray diffraction, and X-ray photoelectron spectroscopy to explore their structures and morphologies. The Bi/Bi_2O_3/PCCs modified glass carbon electrodes were used to simultaneously detect dopamine (DA) and uric acid (UA). The sensors presented preferable sensing performance with wide linear range of 1μM - 50μM for DA and 30μM to 1500μM for UA. The sensitivity and determination limit are 204.38 $\mu A \cdot mM^{-1} \cdot cm^{-2}$ and 0.36 μM for DA and 119.03 $\mu A \cdot mM^{-1} \cdot cm^{-2}$ and 10 μM for UA, respectively. The enhanced electrochemical performance of Bi/Bi_2O_3/PCCs may be due to the synergistic effect of Bi/Bi_2O_3 and porous carbon, where metallic Bi and porous carbon can improve the electron/electrolyte transfer efficiency and provide more active sites for DA and UA oxidation. The Bi/Bi_2O_3/PCCs sensors also presented the good selectivities for DA and UA detection. The as prepared material may be a promising electrocatalyst for biomolecules analysis.

Keywords: Porous carbon; Bismuth; Sensor; Dopamine; Uric acid

1. INTRODUCTION

Sensitively and accurately monitoring biomolecules such as dopamine (DA) and uric acid (UA) is of great importance because they associate with specific diseases[1]. For instance, Alzheimer's and Parkinson's diseases related neurological disorders are greatly regard to the abnormality of the DA level in physiological fluids[2, 3]. As the metabolic product of purine, UA is considered as another important biomarker in blood and urine for clinical diagnosis and healthcare, the abnormality of which might result

in serious diseases including Lesh-Nyhan syndrome, Hyperuricemia, and Gout[4, 5]. Due to the fact that DA is always coexisting with high level of UA, the simultaneous determination of both biomolecules is very important in diagnosing diseases and biomedical chemistry. Various methods including spectrophotometry[6], chemiluminescence[7], liquid chromatography[8], and capillary electrophoresis[9] have been applied to detect DA and UA. Recently, electrochemical sensors were considered as the most promising techniques for DA and UA detection due to the advantages of high sensitivity, easy operation, low cost, and instant analysis[10-12]. Due to the similar oxidation potentials of DA and UA their oxidation peaks are easily overlapped. Thus, electrode materials are greatly vital for the simultaneous determination of DA and UA. Therefore, various nanostructured materials were developed to construct electrochemical sensors for DA and UA detection.

Currently, transition metal-based materials have attracted more and more attentions in developing biosensor as they possess more advantages (such as low cost, more abundance, and better biocompatibility) comparing with noble metals. For instance, nano-hexagonal Fe_2O_3 displayed superior sensing performance for UA and DA detection[13]. g-C_3N_4/Co nanohybrids demonstrated excellent electrocatalytic activities for DA and UA oxidation[14]. Particularly, bismuth-based materials were studied more intensively in biosensing areas own to their ionic conductivity and stability. Such as bismuth molybdates were used as DA sensors displaying excellent electrochemical performance towards DA oxidation[15]. Electrodeposited copper bismuth oxides also demonstrated impressive sensing properties for UA detection[16]. Unfortunately, the sensing performance (such as linear range and sensitivity) of bismuth-based materials still needs to be improved due to the massive aggregation and the poor intrinsic conductivity. Notably, coupling carbon materials (especially the porous carbon) with metal catalysts can greatly improve their electrochemical sensing properties as the porous structures may provide more effective surface area and prevent the agglomeration of catalysts and the high conductivity of carbon materials can improve the charge transfer of the sensors[17-19]. Moreover, the incorporation of metallic Bi on Bi_2O_3 may not only enhance the electronic conductivity and but also produce more redox active sites in the complex materials[20, 21]. Bismuth metal-organic framework, such as Bi-MOF composed of Bi^{3+} and 1,3,5-benzenetricarboxylic acid has a novel porous two-dimensional framework. Due to their inherent large surface area and abundant unsaturated active sites the Bi-MOF derived materials may display superior electrochemical performance[22, 23]. However, to the best of our knowledge, no efforts were attempted to incorporate metallic Bi and Bi_2O_3 on the porous carbon cuboids (PCCs) using Bi-MOF as precursors for simultaneous determination of dopamine and uric acid.

Herein, we report the in situ generation of Bi/Bi_2O_3 on PCCs through pyrolyzing the bismuth based metal organic frameworks (Bi-MOFs) under inert atmosphere. The as prepared materials were investigated by cyclic voltammetry (CV) and differential pulse voltammetry (DPV) to evaluate their sensing performance for UA and DA detection. The sensors displayed high sensitivities and wide linear ranges for simultaneously detecting DA and UA. The superior sensing properties may be due to the synergistic effects of metallic Bi, Bi_2O_3 and porous structured carbon cuboids, which may provide more active sites and improve the charge transfer efficiency.

2. EXPERIMENTAL SECTION

2.1 Preparation of Bi/Bi_2O_3/PCCs

Bi/Bi_2O_3/PCCs were obtained by pyrolyzing cuboid structured Bi-MOFs in N_2 atmosphere. Firstly, 4.85g $Bi(NO_3)_3 \cdot 5H_2O$ and 4.203g 1,3,5-Benzenetricarboxylic Acid were evenly grinded and then transferred into 100 ml methanol. The mixed solution was stirred at 60 ºC for 4 h. The precipitates of Bi-MOFs were achieved by successively centrifuging at 4000r/min, washing with methanol, and drying at 60 ºC overnight. The Bi/Bi_2O_3 coupled porous carbon cuboids (Bi/Bi_2O_3/PCCs) were obtained by annealing the precipitate at 800 ºC for 2 h under N_2 atmosphere with the heating rate of 5 ºC/min. As a comparison, the precipitate was also annealed with the same procedure at the air atmosphere instead of N_2 atmosphere, which was labelled as Bi_2O_3.

2.2 Materials characterization

XRD was carried out on Thermo ARL SCINTAG X'TRA. SEM was performed in a Hitachi S-4700 and XPS analysis was measured on a PHI-5400 system. Electrocatalysts were evaluated on CHI630D and Zahner Zennium work stations.

2.3 Electrochemical Measurements

All the electrochemical measurements were conducted with a three-electrode configuration using 0.1M phosphate buffer solution (PBS) as supporting electrolyte. Saturated calomel electrode and Pt plate electrode are reference and counter electrodes. Glassy carbon electrodes (GCEs) were modified by the obtained catalysts and used as working electrodes. Typically, GCEs were firstly polished with 0.3μm alumina and then rinsed with deionized water and ethanol and dried in air. Subsequently, 10 μL catalyst slurry (8mg catalysts, 10ml ethanol and 10 μL Nafion solution) was dropped onto the glass carbon area and dried in air. CVs were recorded at the potentials ranging from -0.1 V to 0.6 V with scan rate of 50 mV/s. DPVs were measured from -0.1 V to 0.6 V with step potential of 4 mV, the amplitude of 50 mV and pulse width of 0.04 s and pulse period of 0.5 s. The interference study of DPVs were investigated in the same procedures in 0.1 M PBS in presence of different interferents (Such as urea, glucose, proline, lysine, glutamate, and valine). The frequency in electrochemical impedance spectroscopy (EIS) measurement was set as 10 mHz - 100KHz with the amplitude of 5 mV.

3. RESULTS AND DISCUSSION

Fig. 1 displays the morphology of the obtained materials. The SEM images of Bi-MOFs (Fig. 1a and b) demonstrate typical cuboids-like structures with relatively smooth surface. After annealing at 800 ºC the surface of Bi/Bi_2O_3/PCCs (Fig. d, e, f) turned much rougher than that of Bi-MOF. The similar cuboids-structures can also be observed on Bi/Bi_2O_3/PCCs, which exhibited distinct porous structures and overlapped with each other with random aggregations of nanoparticles. The distinctly bright

nanoparticles may be metallic Bi or Bi_2O_3 originating from Bi^{3+} in Bi-MOFs. The EDS pattern (Fig. 2a) proves the existence of Bi, O and C elements in Bi/Bi_2O_3/PCCs. The elemental mapping further demonstrates the uniform distribution of Bi, O and C in the sample, which may suggest the even dispersion of Bi/Bi_2O_3 in the entire cuboids-like structures of Bi-MOFs derived carbon. XRD (Fig. 2b) analysis proves the existence of both metallic Bi and Bi_2O_3 in Bi/Bi_2O_3/PCCs. The diffraction signals corresponding to (201), (002), (220), (222), (400), (203), (421), (402), and (610) crystal planes of tetragonal Bi_2O_3 can be observed on the XRD patterns (PDF#27-0050). Moreover, the diffraction peaks marked with asterisks can be indexed to hexagonal Bi (PDF#44-1246). The results may indicate that Bi/Bi_2O_3 were successfully generated on the PCCs.

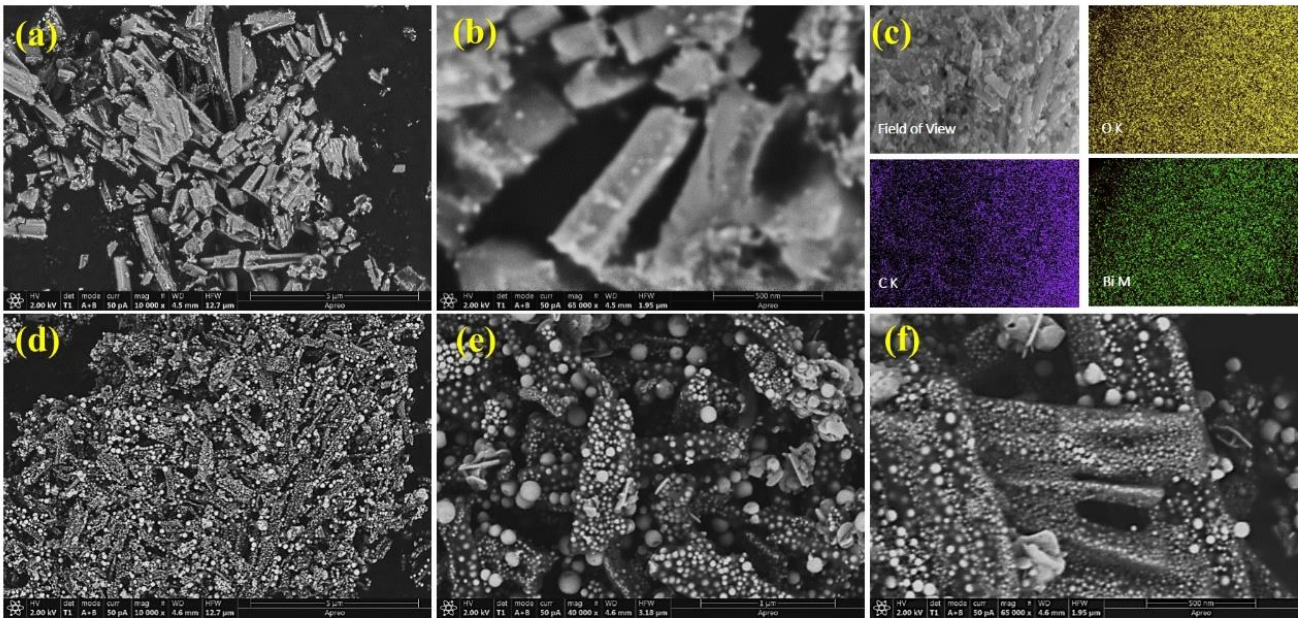

Figure 1. SEM images of Bi-MOF (a, b) and Bi/Bi_2O_3/PCCs (d, e, f); (c) Elemental mapping of Bi/Bi_2O_3/PCCs.

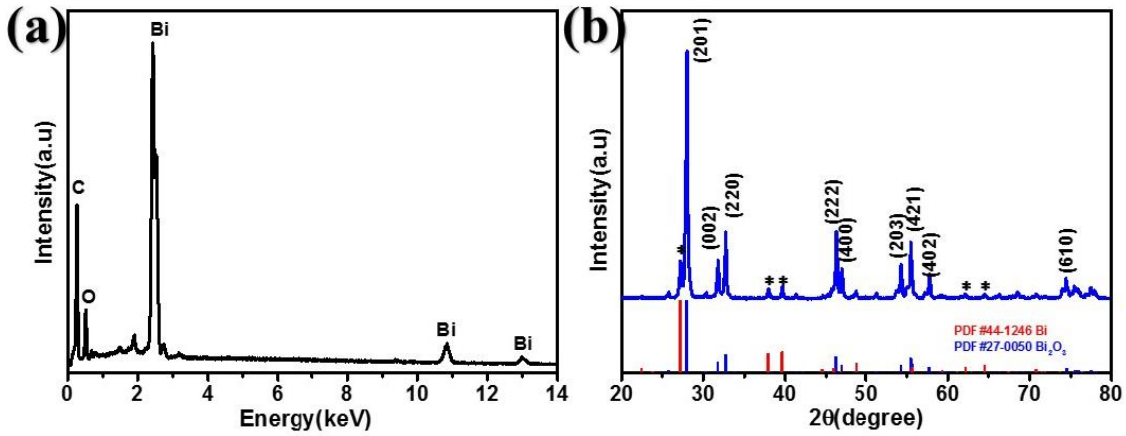

Figure 2. (a) EDS spectra of Bi/Bi_2O_3/PCCs; (b) XRD pattern of Bi/Bi_2O_3/PCCs.

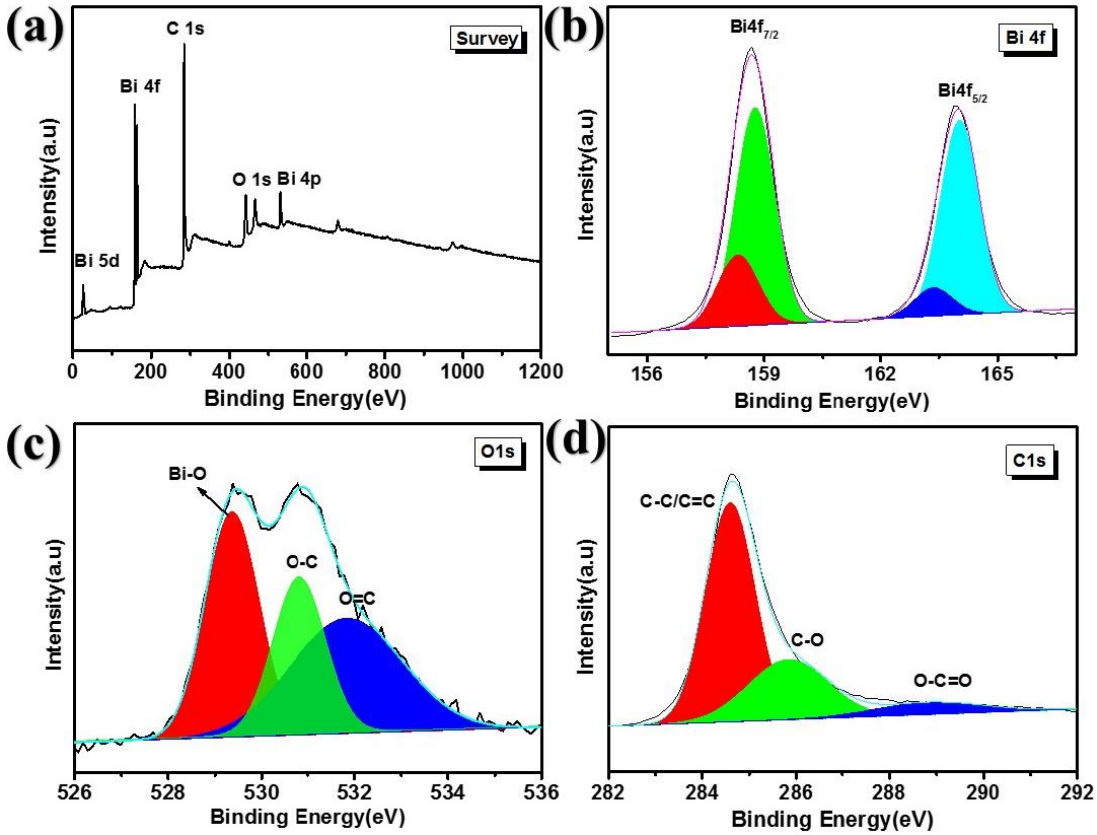

Figure 3. XPS survey spectra (a) and Bi 4f (b), O 1s (c), and C 1s (d) spectra of Bi/Bi_2O_3/PCCs.

The valence state and composition of Bi/Bi_2O_3/PCCs were further evaluated by XPS. Distinct signals of Bi, O and C can be investigated on the XPS survey spectra (Fig. 3a), indicating the successful formation of Bi/Bi_2O_3/PCCs, which is consistent with the EDS results. Bi 4f spectrum (Fig. 3b) can be deconvoluted into two pairs of Bi 4f peaks suggesting the existence of two different states of Bi. The peaks at 158.8 eV and 164.03 eV can be attributed to the Bi^{3+} 4f 7/2 and Bi^{3+} 4f 5/2 corresponding to Bi^{3+} in Bi_2O_3 and another two peaks are related to the metallic Bi[24, 25]. Three peaks can be observed on the deconvoluted O 1s XPS spectrum (Fig. 3c). The peaks located at 529.4 eV corresponds to the Bi-O bond in Bi_2O_3 and another two may be attributed to the adsorbed oxygen (O-C/O=C) on the surface of Bi/Bi_2O_3/PCCs [26, 27]. C 1s spectrum is showed in Fig. 3d, which presents three peaks of C-C/C=C (284.6 eV), C-O (285.8 eV), and O-C=O (288.8 eV), respectively, suggesting the formation of PCCs. The XPS results further confirmed the successful synthesis of the Bi/Bi_2O_3/PCCs electrocatalysts.

CVs were carried out in 0.1M PBS (pH 7.5) to evaluate the electrochemical performance of electrodes. Both CVs of Bi/Bi_2O_3/PCCs and Bi_2O_3 electrodes (Fig. 4a) displayed no detectable anodic peaks in PBS and the current of Bi/Bi_2O_3/PCCs is much higher than that of Bi_2O_3 electrodes, indicating better electrocatalytic activity of Bi/Bi_2O_3/PCCs. The electrocatalytic oxidation of 20 μM DA (Fig. 4b) and 300 μM UA (Fig. 4c) were also investigated on both Bi/Bi_2O_3/PCCs and Bi_2O_3 electrodes. Distinct anodic peaks can be observed on both CV curves of Bi/Bi_2O_3/PCCs implying that they have good catalytic activities for DA and UA oxidation. Fig. 4d demonstrates the CVs of Bi/Bi_2O_3/PCCs and Bi_2O_3 electrodes simultaneously in presence of both DA and UA. Although the anodic peaks are not as obvious

as individual measurement, the highly increased anodic currents for both DA and UA oxidation can also be investigated on Bi/Bi_2O_3/PCCs electrodes, suggesting the improved sensing performance for simultaneously DA and UA detection.

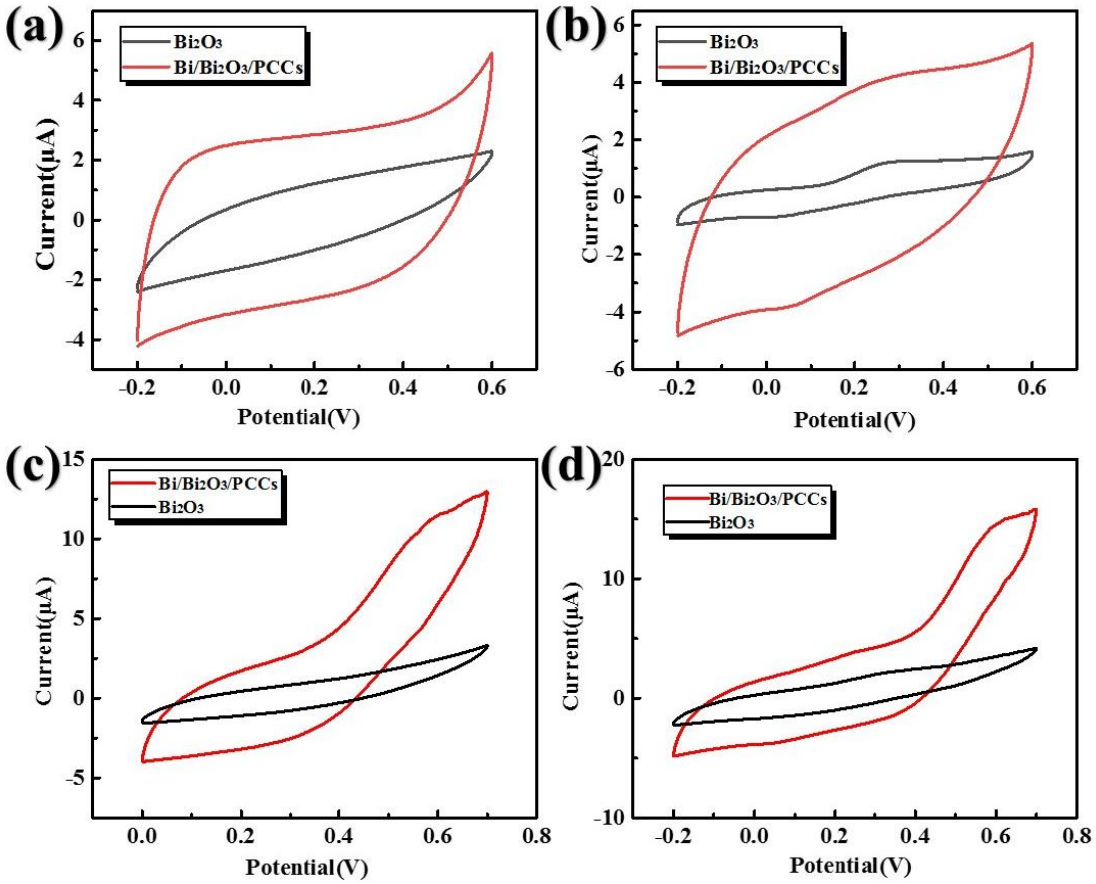

Figure 4. CVs of Bi/Bi_2O_3/PCCs and Bi_2O_3 recorded in 0.1 M PBS (pH 7.4) without (a) and with 20 μM DA (b), 300 μM UA (c), and mixture of 20 μM DA and 300 μM UA (d).

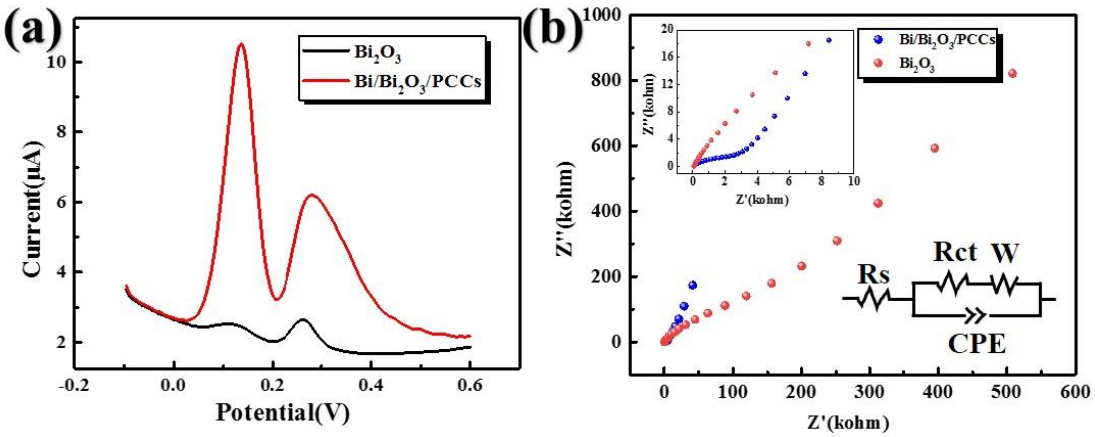

Figure 5. (a) DPVs of Bi/Bi_2O_3/PCCs and Bi_2O_3 in presence of 40 μM DA and 100 μM UA; (b) EIS spectra of Bi/Bi_2O_3/PCCs and Bi_2O_3 in 0.1 M PBS (pH 7.4) (inset of upper left is the enlarged EIS in high frequency and bottom right is the equivalent electrical circuit).

DPV is a highly sensitive analytical method because it can effectively inhibit the influence of charging current. Therefore, DPV method was applied to investigate the current sensitivity and separative capacity for DA and UA detection. Fig. 5a shows the DPV curves of Bi/Bi_2O_3/PCCs and Bi_2O_3 electrodes with a mixture of 40 μM DA and 100 μM UA in 0.1 M PBS. Two distinguished peaks with peak separation of 0.145 V can be observed on Bi/Bi_2O_3/PCCs, suggesting they have preferable capability for simultaneous detection of DA and UA. Moreover, the peak currents for DA and UA oxidation on Bi/Bi_2O_3/PCCs are much higher (4.2 times for DA and 2.3 time for UA) than that of Bi_2O_3, indicating the better sensing performance of Bi/Bi_2O_3/PCCs. The interfacial conductivity was evaluated by EIS to further explore the improvement of the sensing performance on Bi/Bi_2O_3/PCCs electrodes. As can be investigated on Fig. 5b, EIS of both Bi/Bi_2O_3/PCCs and Bi_2O_3 electrodes present compressed semicircles in higher frequency and relatively straight line in lower frequency, which are related to the charge transfer resistance (Rct) and electron/electrolyte diffusion (W), respectively. The diameter of semicircles for Bi/Bi_2O_3/PCCs is much lower than that of Bi_2O_3, implying the lower Rct (2.94×10^3 Ω vs. 1.35×10^5 Ω obtained from the corresponding equivalent circuit) and faster charge transfer efficiency of Bi/Bi_2O_3/PCCs. The lower Rct of Bi/Bi_2O_3/PCCs may be due to the incorporation of metallic Bi and the combination of porous carbon cuboids. The results suggest that Bi/Bi_2O_3/PCCs may possess better electrochemical activities for UA and DA oxidation, which is consistent with CVs and DPV analysis.

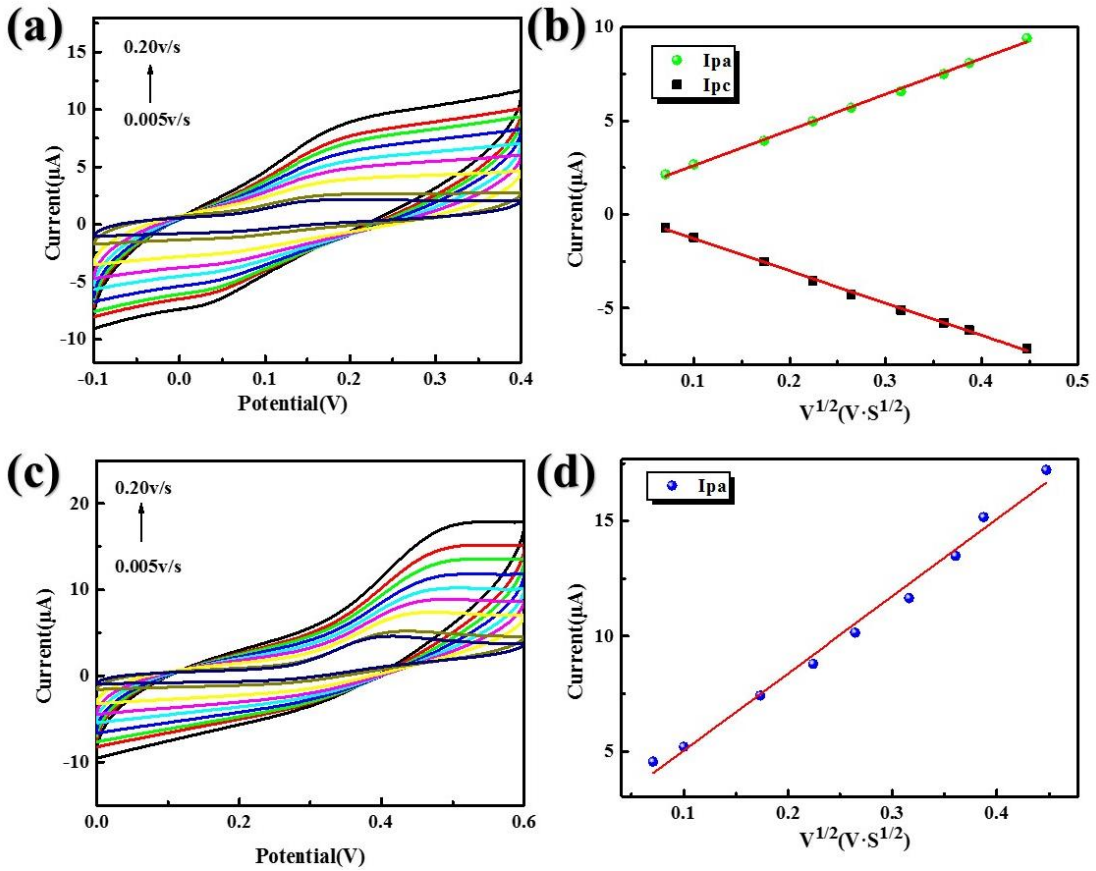

Figure 6. CVs of Bi/Bi_2O_3/PCCs in presence of 50 μM DA (a) and 300 μM UA (c) with various scan rates; the linear plots between square root of scan rates and current response of DA (b) and UA (d).

The kinetics of DA and UA oxidation on Bi/Bi_2O_3/PCCs electrodes were also investigated by recording CVs with various scan rate (ν) in 0.1 PBS. As can be observed on Fig. 6a redox peak currents for DA oxidation increased gradually with ν increasing. Moreover, the slight shift of anodic and cathodic peaks to higher and lower potentials indicates the kinetic limitation for DA electrocatalytic oxidation. The plots of anodic and cathodic peak currents (I_{pa} and I_{pc}) vs. $\nu^{1/2}$ (Fig. 6b) demonstrates a good linear relationship in a wide range (0.005 V/s - 0.2V/s), suggesting the diffusion-controlled process for DA oxidation on Bi/Bi_2O_3/PCCs electrodes[13, 28]. The CVs of Bi/Bi_2O_3/PCCs electrodes for UA oxidation (Fig. 6c) displays distinct anodic peaks and indistinct cathodic peaks in all the scan range (0.005 V/s - 0.2V/s), implying the irreversible oxidation of UA on electrodes. Moreover, the I_{pa} also increased with the increase of ν. The good linear relationship was also obtained between I_{pa} and $\nu^{1/2}$ (Fig. 6d), which also indicates the diffusion-controlled reaction for UA oxidation. Therefore, the reaction of both UA and DA oxidation on the surface of Bi/Bi_2O_3/PCCs are diffusion-controlled process.

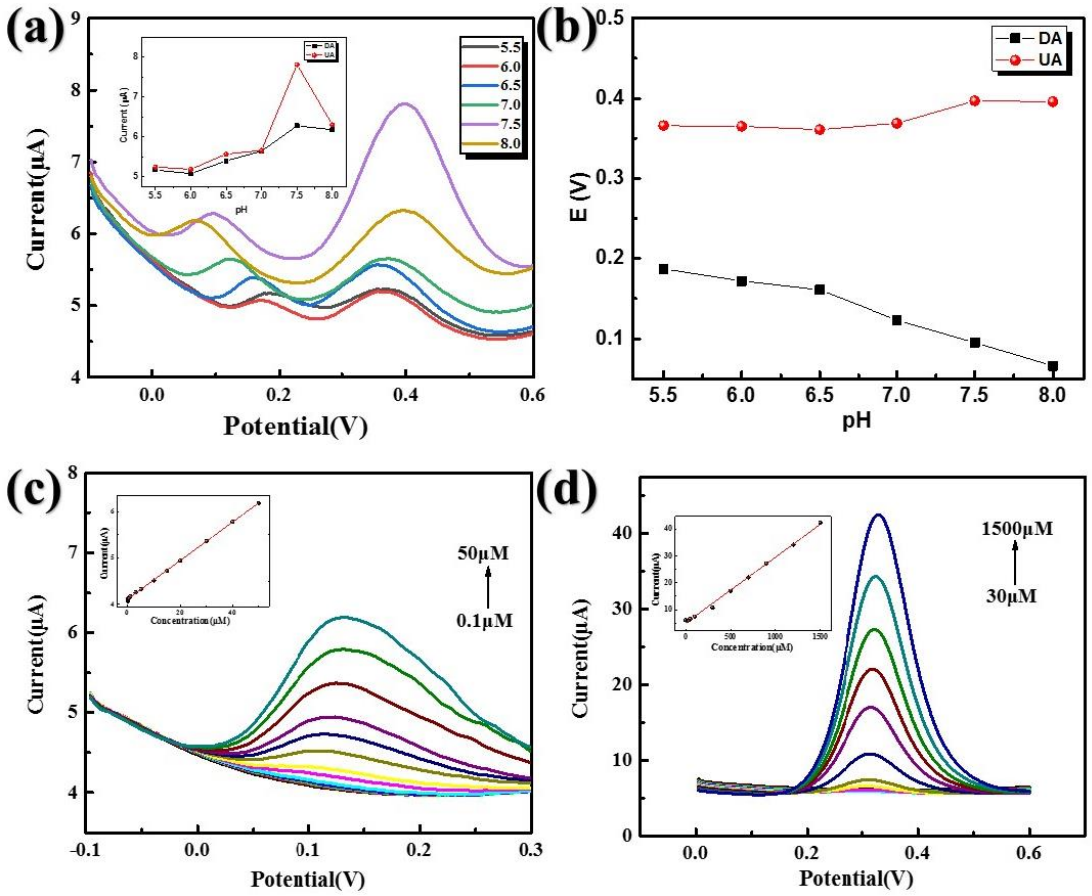

Figure 7. (a) DPVs of Bi/Bi_2O_3/PCCs in presence of 40 μM DA and 200 μM UA with various pH (Insert is the effects of pH on anodic currents of DA and UA); (b) Effects of pH on anodic peak potentials of DA and UA; DPVs of Bi/Bi_2O_3/PCCs in 0.1 M PBS (pH 7.5) with various DA (c) and (UA) (Inserts are the corresponding linear plots between anodic currents and concentration of DA and UA).

The sensing performance for UA and DA detection can be greatly affected by the pH of supporting electrolytes. The DPV curves of Bi/Bi_2O_3/PCCs electrodes (Fig. 7a) were recorded in presence of 40 μM DA and 200 μM UA with various pH. It can be observed (insert in Fig. 7a) that both DA and UA displayed an increase of peak currents with pH increasing from 5.5 to 7.5. However, the subsequent increase of pH resulted in the distinct decrease of peak currents. Fig. 7b demonstrates the peak separation of DA and UA with different pH, implying that the higher pH is beneficial to the peak separation. Considering the comprehensive impact of pH to peak potentials and currents, all the subsequent DPV measurements were performed in PBS with pH of 7.5.

Individual detection of UA and DA with Bi/Bi_2O_3/PCCs electrodes was investigated by recording DPV curves in pH 7.5 PBS with various concentration of DA and UA. As shown in Fig. 7c the anodic current response of DA increases distinctly with increasing concentration of DA. The good linear relationship between DA concentration (1 μM - 50 μM) and current response can be obtained from the linear regression equation of I_{ap} (μA) = 0.04161 C (μM) + 4.1137 (μA) (R^2 = 0.99945) (Insert in Fig. 7c). The detection limit (LOD) of DA can be calculated to be 0.33 μM (S/N = 3) and the sensitivity is 212.03 $\mu A \cdot mM^{-1} \cdot cm^{-2}$. Fig. 7d demonstrates the DPV of UA with concentration ranging from 30μM to 1500μM, which presents the similar relationship between I_{ap} and C_{UA}. The linearity was described as I_{ap} (μA) = 0.02456 C (μM) + 5.0349 (μA) (R^2 = 0.99709) with sensitivity of 125.15 $\mu A \cdot mM^{-1} \cdot cm^{-2}$ and LOD of 10 μM.

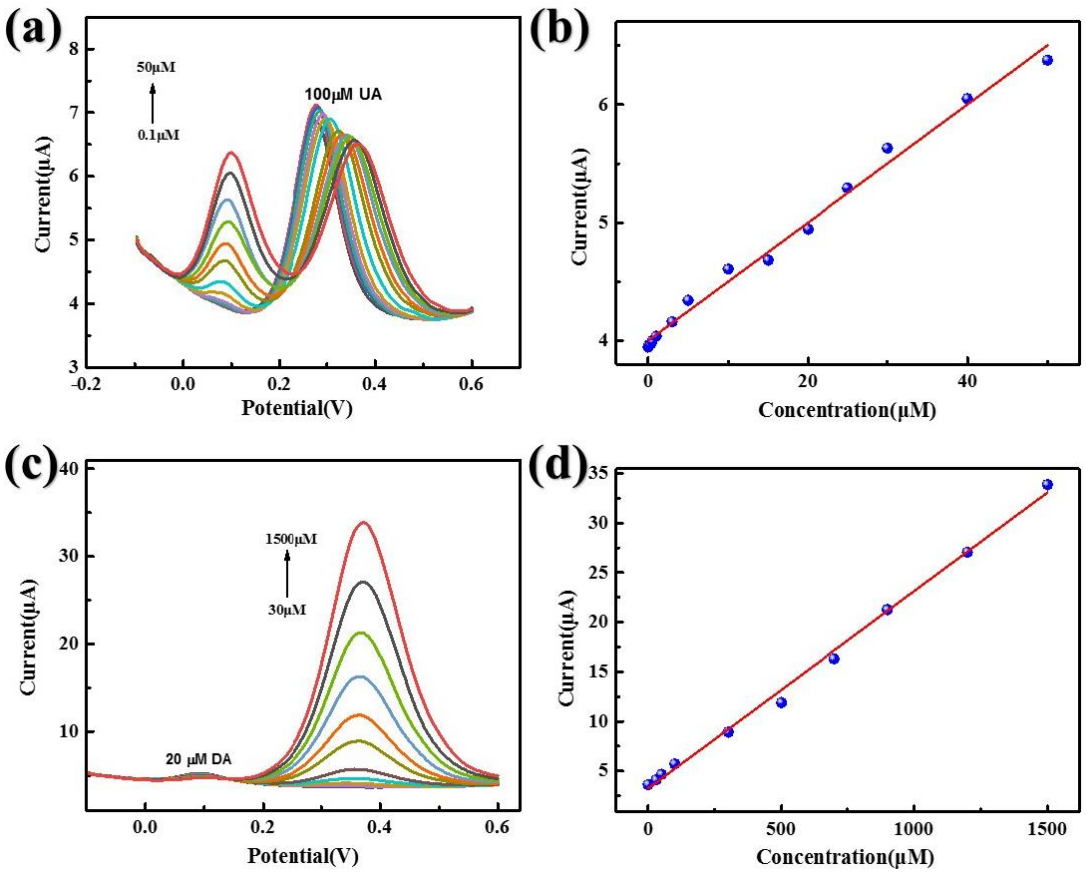

Figure 8. DPVs of Bi/Bi_2O_3/PCCs in 0.1 M PBS (pH 7.5) for (a) various DA with fixed concentration of UA and (c) various UA with fixed DA; The corresponding plots of anodic currents vs. concentration of (b) DA and (d) UA.

Apart from the preferable individual sensing properties for UA and DA detection on Bi/Bi_2O_3/PCCs electrodes, the sensors were also evaluated by DPV to analyze UA and DA with the fixed concentration of DA and UA, respectively. Fig. 8a displays the DPV curves of DA on Bi/Bi_2O_3/PCCs electrodes in presence of 100 μM UA. It can be observed that with the increase of DA concentration anodic current increases gradually and UA has no effect on the DA detection. The linear regression of DA (Fig. 8b) is I_{ap} (μA) = 0.05006 C (μM) + 3.99957 (μA) (R^2 = 0.99192) in range of 0.5μM - 50μM. The LOD and sensitivity are 0.17μM and 255.08 $\mu A \cdot mM^{-1} \cdot cm^{-2}$, respectively. Similar trends can also be observed when fixing DA concentration and increasing UA concentration from 30μM to 1500μM (Fig. 8c). Linear plots between I_{pa} and C_{UA} are illustrated in Fig. 8d with regression equation of I_{ap} (μA) = 0.01988 C (μM) + 3.24251 (μA) (R^2 = 0.99626). The LOD and sensitivity are 10 μM and 101.30 $\mu A \cdot mM^{-1} \cdot cm^{-2}$, respectively. The results suggest that the Bi/Bi_2O_3/PCCs electrodes may have preferable sensing performance for simultaneous detection of UA and DA.

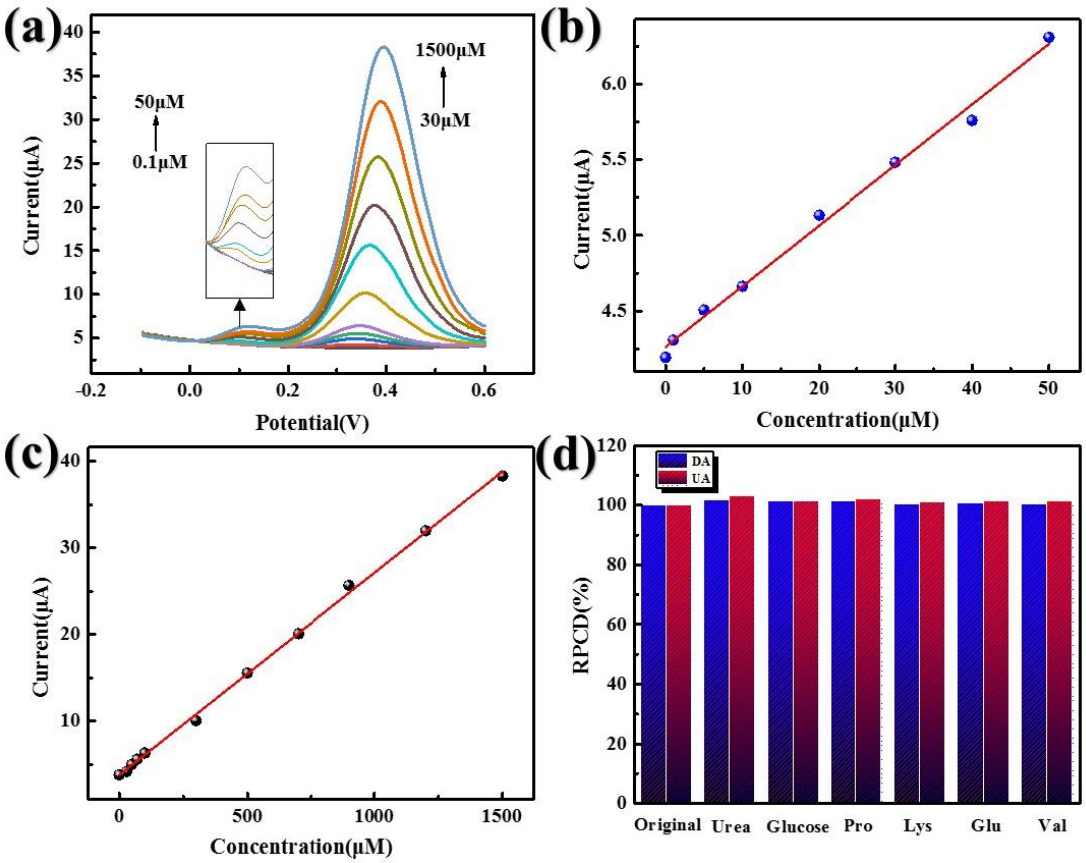

Figure 9. (a) DPVs of Bi/Bi_2O_3/PCCs in 0.1 M PBS (pH 7.5) with various concentration of DA and UA; The corresponding plots of anodic currents vs. concentration of DA (b) and UA (c); (d) anodic current response of Bi/Bi_2O_3/PCCs in presence of various interferents.

Moreover, the simultaneous detection of both UA and DA on Bi/Bi_2O_3/PCCs sensors was also investigated by recording DPV response with simultaneously increasing DA and UA concentration. Fig.

9a demonstrates two well-defined peaks corresponding to DA and UA oxidation and the separated peak currents increase with increasing the concentration of two compounds. The linear range of DA is 1μM - 50μM with the regression equation of I_{ap} (μA) = 0.04011 C (μM) + 4.26153 (μA) (R^2 = 0.995) (Fig. 9b). The LOD is about 0.36 μM and the sensitivity is 204.38 $\mu A \cdot mM^{-1} \cdot cm^{-2}$, which is close to the value obtained with fixed UA concentration (255.08 $\mu A \cdot mM^{-1} \cdot cm^{-2}$) and with absence of UA (212.03 $\mu A \cdot mM^{-1} \cdot cm^{-2}$). The fitting results of UA (Fig. 9c) also present the similar results with the regression equation of I_{ap} (μA) = 0.02336 C (μM) + 3.78672 (μA) (R^2 = 0.99881) and linear range of 30μM - 1500μM. Moreover, the sensitivity of 119.03$\mu A \cdot mM^{-1} \cdot cm^{-2}$ with LOD of 10 μM is close to 101.30 $\mu A \cdot mM^{-1} \cdot cm^{-2}$ (fixed DA) and 125.15 $\mu A \cdot mM^{-1} \cdot cm^{-2}$ (without DA). The results suggested the independent oxidation of UA and DA on the Bi/Bi_2O_3/PCCs electrode, which is possible for simultaneously detecting both compounds without any mutual interference. The sensing performance of Bi/Bi_2O_3/PCCs sensors has also been compared with the previously reported electrochemical sensors (Table 1). The Bi/Bi_2O_3/PCCs sensors displayed relatively wider linear range and lower detection limit.

Table 1. Comparison of the sensing performance of the Bi/Bi_2O_3/PCCs sensors with other electrochemical sensors

Electrode materials	**Linear range (μM)**		**LOD (μM)**		**Reference**
	DA	**UA**	**DA**	**UA**	
Bi/Bi_2O_3/C	0.1-50	30-1500	0.03	10	This work
Au-Cu_2O/rGO	10-90	100-900	3.9	6.5	[29]
N-rGO	1-60	1-30	0.1	0.2	[30]
MnO_2/NG	0.1-10	10-100	0.034	0.039	[31]
NiO-trGO	10-500	100-500	0.05	10	[32]
GO/$TmPO_4$	2-20	10-100	0.785	3.73	[33]
AuNPs@ACOF/p-BFu	0.75-40	1-200	0.15	0.22	[34]
3D-KSC/C_{CSBP}	14.1-100	450-1200	4.6	150	[35]

Table 2. determination results of DA in serum sample

Sample	**Added(μM）**	**Found(μM)**	**Recovery(%)**
1	10.00	10.14	101.4
2	20.00	20.42	102.1
3	30.00	32.02	106.7

Table 3 determination results of UA in serum sample

Sample	**Added(μM）**	**Found(μM)**	**Recovery(%)**
1	100.00	101.21	101.2
2	200.00	204.88	102.4
3	300.00	303.23	101.1

The selectivity of Bi/Bi_2O_3/PCCs sensors was also investigated by recording DPVs of UA (40μM) and DA (300 μM) in presence of various interferences such as Urea, Glucose, Pro, Lys, Glu, and Val. The current responses of UA and DA with the coexistence of interferences are showed in Fig. 9d. As can be found that the interfering substances have no distinct effect on simultaneous detection of DA and UA. Therefore, the results may suggest that the Bi/Bi_2O_3/PCCs sensors have preferable selectivity for UA and DA analysis. DA and UA in real serum samples were also detected by DPVs with a standard addition method to demonstrate the applicability of Bi/Bi_2O_3/PCCs sensors. Table 2 and 3 display that the recoveries of the DA are in the range of 101.4% - 106.75% and the recoveries of UA are between 101.1% and 102.4%, which are within the reasonable ranges. The results suggested that the Bi/Bi_2O_3/PCCs sensors can also be used to detect UA and DA in real samples with good accuracy and high precision.

4. CONCLUSION

In summary, Bi/Bi_2O_3/PCCs were prepared through pyrolyzing Bi-MOF with organic frameworks as both carbon source and reducing agent to form the metallic Bi. The obtained Bi/Bi_2O_3/PCCs were applied to simultaneously detect DA and UA, which presents excellent sensing performance including high sensitivity and low detection limit. The linear range of DA detection is 1μM - 50μM with sensitivity and LOD of 204.38 $\mu A \cdot mM^{-1} \cdot cm^{-2}$ and 0.36 μM, respectively. The linear range of UA ranges from 30 μM to 1500 μM with sensitivity and LOD of 119.03 $\mu A \cdot mM^{-1} \cdot cm^{-2}$ and 10 μM, respectively. The improved sensing performance of Bi/Bi_2O_3/PCCs may be due to the faster charge transfer efficiency originating from the incorporation of metallic Bi and the combination of porous carbon cuboids. Therefore, the study of Bi/Bi_2O_3/PCCs sensor may provide a promising strategy to construct new sensing materials for biomolecules detection.

ACKNOWLEDGMENTS
Authors would like to thank the support from the foundation of Zhejiang natural science (No. Y19E060021).

References

1. Q. He, J. Liu, J. Liang, X. Liu, W. Li, Z. Liu, Z. Ding, D. Tuo, *Cells*, 7 (2018) 24.
2. M. D'Amelio, S. Puglisi-Allegra, N. Mercuri, *Pharmacol. res*., 130 (2018) 414.
3. N.X. Tritsch, B.L. Sabatini, *Neuron*, 76 (2012) 33.
4. M.K. Kutzing, B.L. Firestein, *J. Pharmacol. Exp. Ther*., 324 (2008) 1.
5. R. El Ridi, H. Tallima, *J. adv. res.*, 8 (2017) 487.
6. H. Khajehsharifi, E. Pourbasheer, H. Tavallali, S. Sarvi, M. Sadeghi, *Arab. J. Chem*., 10 (2017) S3451.
7. Y. Lan, F. Yuan, T.H. Fereja, C. Wang, B. Lou, J. Li, G. Xu, *Anal. chem*., 91 (2018) 2135.
8. L. Das, S. Das, A.C. Ir, A.K. Mallick, A. Gupta, *J. Chromatogr*. B, 1180 (2021) 122894.
9. A. Roychoudhury, K.A. Francis, J. Patel, S.K. Jha, S. Basu, *RSC Adv*., 10 (2020) 25487.
10. R. Zainul, N. Hashim, S.N.A.M. Yazid, S.N.M. Sharif, M.S. Ahmad, M.I. Saidin, S. Suyanta, M. Sobry, I.M. Isa, *Int. J. Electrochem. Sci*., 16 (2021) 1.

11. C. Nong, B. Yang, X. Li, S. Feng, H. Cui, *Int. J. Electrochem. Sci*., 17 (2022).
12. W. Wang, F. Wei, B. Han, *Int. J. Electrochem. Sci*, 17 (2022) 2.
13. M.Y. Emran, M.A. Shenashen, A.A. Abdelwahab, M. Abdelmottaleb, M. Khairy, S.A. El-Safty, *Electrocatalysis*, 9 (2018) 514.
14. M. Wang, M. Zhang, J. Zhu, J. Wang, L. Hu, T. Sun, M. Wang, Y. Tang, *ChemElectroChem*, 7 (2020) 1373.
15. S. Maheshwaran, E. Tamilalagan, S.-M. Chen, M. Akilarasan, Y.-F. Huang, N. AlMasoud, K.M. Abualnaja, M. Ouladsmne, *Microchim. Acta*, 188 (2021) 1.
16. G.N. Sinha, P. Subramanyam, V. Sivaramakrishna, C. Subrahmanyam, *Inorg. Chem. Commun*., 129 (2021) 108627.
17. H. Yu, J. Jiang, Z. Zhang, G. Wan, Z. Liu, D. Chang, H. Pan, *Anal. biochem*., 519 (2017) 92.
18. W. Yao, H. Guo, H. Liu, Q. Li, N. Wu, L. Li, M. Wang, T. Fan, W. Yang, *Microchem. J*., 152 (2020) 104357.
19. Y. Chen, X. Zhang, A. Wang, Q. Zhang, H. Huang, J. Feng, *Microchim. Acta*, 186 (2019) 1.
20. T. Qin, D. Wang, X. Zhang, Y. Wang, N.E. Drewett, W. Zhang, T. Dong, T. Li, Z. Wang, T. Deng, Z. Pan, N. Yue, R. Yang, K. Huang, S. Feng, R. Huang, W. Zheng, *Energy Storage Mater*., 36 (2021) 376.
21. H. Wu, J. Guo, D.a. Yang, *J. Mater. Sci. Technol*., 47 (2020) 169.
22. Z. Wang, Z. Zeng, H. Wang, G. Zeng, P. Xu, R. Xiao, D. Huang, S. Chen, Y. He, C. Zhou, M. Cheng, H. Qin, *Coordin. Chem. Rev*., 439 (2021) 213902.
23. Y. Zhou, R. Abazari, J. Chen, M. Tahir, A. Kumar, R.R. Ikreedeegh, E. Rani, H. Singh, A.M. Kirillov, *Coordin. Chem. Rev*., 451 (2022) 214264.
24. Y. Zhao, X. Qin, X. Zhao, X. Wang, H. Tan, H. Sun, G. Yan, H. Li, W. Ho, S. Lee, Chinese. *J. Catalysis*, 43 (2022) 771.
25. J. Qin, S. Ye, K. Yan, J. Zhang, *J. Colloid. Interf. Sci*., 607 (2022) 1936.
26. N. Sun, B. Yin, D. Dong, X. Hu, Y. Huan, T. Wei, *Electrochim. Acta*, 409 (2022) 139948.
27. M. Chahkandi, M. Zargazi, A. Hajizadeh, R. Tayebee, *J. Alloy. Compd*., 902 (2022) 163737.
28. A.S. Ahammad, N. Odhikari, S.S. Shah, M.M. Hasan, T. Islam, P.R. Pal, M.A.A. Qasem, M.A. Aziz, *Nanoscale Adv.*, 1 (2019) 613.
29. T.K. Aparna, R. Sivasubramanian, M.A. Dar, *J. Alloy. Compd*., 741 (2018) 1130.
30. H. Zhang, S. Liu, *J. Alloy. Compd*., 842 (2020) 155873.
31. Q. Li, Y. Xia, X. Wan, S. Yang, Z. Cai, Y. Ye, G. Li, *Mat. Sci. Eng. C*, 109 (2020) 110615.
32. T. Aparna, R. Sivasubramanian, *J. Nanosci. Nanotechno*., 18 (2018) 789.
33. H. Huang, Y. Yue, Z. Chen, Y. Chen, S. Wu, J. Liao, S. Liu, H. Wen, *Microchim. Acta*, 186 (2019) 1.
34. Y. He, X. Lin, Y. Tang, L. Ye, *Anal. Methods-UK*., 13 (2021) 4503.
35. X. Peng, Y. Xie, Y. Du, Y. Song, S. Chen, *J. Electroanal. Chem*., 904 (2022) 115850